

Full-Body Visible Human Project[®] Female Computational Phantom and Its Applications for Biomedical Electromagnetic Modeling

J. Yanamadala, V. K. Rathi, S. Maliye, H. A. Win, A. L. Tran, M. Zagalskaya, G. M. Noetscher, S. N. Makarov

Electrical and Computer Engineering
Department

Worcester Polytechnic Institute
Worcester, MA 01604, USA
makarov@wpi.edu

M. K. Kozlov
Max Plank Inst. for Human Cognitive
and Brain Sciences
Stephanstraße 1a, 04103 Leipzig,
Germany
kozlov@cbs.mpg.de

A. Nazarian
Beth Israel Deaconess Medical Center
Harvard Medical School
330 Brookline Ave, Boston, MA 02215,
USA
anazaria@bidmc.harvard.edu

Abstract—This study describes the development to date of a computational full-body human phantom based on the VHP female dataset. Its unique feature is full compatibility both with MATLAB and specialized FEM computational software packages such as ANSYS HFSS/Maxwell 3D. Applications for low-frequency and radio-frequency electromagnetic modeling are considered.

Keywords— *Image segmentation; Visible Human Project[®] (VHP); Computational phantom, MATLAB[®]; Low-frequency electromagnetic modeling, RF modeling*

I. INTRODUCTION

The computational phantom disclosed in this study was constructed using anatomical cryosection images taken in the axial plane as provided by the Visible Human Project[®] (VHP) established in 1989 by the U.S. National Library of Medicine (NLM) [1]. Male and female data sets became available in November of 1994 and 1995, respectively. The VHP-Male dataset was segmented at RPI as well as by CST Microwave Studio and REMCOM for commercial purposes. All three phantoms are voxel-based phantoms. The voxel phantoms are not suitable for FEM or MoM frequency-domain analysis. We propose, for the first time, the VHP-Female phantom. Anatomical cryosection image data from the female patient, consisting of 2048 by 1216 pixels with each pixel measuring 0.33mm per side, was used in the construction of the model for the present study, producing the VHP-Female nomenclature. The original VHP-NLM model resolution in the axial plane is 0.33mm by 0.33mm. Since every third image in the dataset was utilized, resolution along the vertical axis of the body is limited to 0.99mm.

II. EARLY SEGMENTATION EFFORTS

Image segmentation is an area of active research with many dynamic and varying methodologies. Despite this diversity in implementation, no one singular technique has proven to be

suitable in all applications or as accurate as manual segmentation by a human operator. Though extremely time consuming, it is for this reason that manual and semi-manual segmentation was employed by our group almost exclusively for the development of the VHP-Female triangular surface meshes.

One of the major tools developed in conjunction with VHP dataset and utilized to create early VHP triangular surface meshes was the open source program Insight Toolkit-SNAP (ITK-SNAP) [2], which enables the analysis of three dimensional image stacks and simultaneous segmentation of images in the axial, coronal, and sagittal body planes via manual and automatic methods. The user may manually trace organs, tissues and other structures, thus isolating these regions from other image areas. The end result is a stereolithography (STL) file describing the surface of the segmented region as a dense triangular mesh (surface Delaunay triangulation) defined by a node point cloud.

Much of the mesh conditioning process has been accomplished via the open source program *MeshLab* [3]. Example operations include selective reduction of the number of nodes via quadric edge collapse decimation [4], surface preserving (HP) Laplacian smoothing [5], Poisson surface reconstruction, [6] etc.

Following the segmentation and conditioning processes, all individual components of the VHP-Female model were registered to ensure proper position, size and shape. Registration was accomplished by overlaying the digitized structures on top of the original cryosection images and any required adjustments were made on a node by node or element by element basis. The resulting surface reconstruction error (deviation of the triangulated surface from the real one) does not exceed 0.5 mm -2 mm within the human head and 5 mm otherwise. The error in the human head is comparable with the state-of-the-art Virtual Family V3.0 models provided by

Foundation for Research on Information Technologies in Society (IT²S) (Switzerland).

The initial VHP-Female model contained 33 individual tissues describing the human head and torso (with superior resolution within the human head, including the continuous CSF shell) [7]. In 2014, this partial model was evaluated and accepted by the IEEE International Committee on Electromagnetic Safety for the calculation of Specific Absorption Rates (SARs) [8].

III. SEGMENTATION IN MATLAB[®]

The latest basic MATLAB platform (without toolboxes) has a number of built-in and open-source features that make it an accessible alternative for medical image segmentation and surface reconstruction. These features relate to both computational geometry and image processing. In particular, they include (compatibility with R2015a):

- Pixel-based image processing tools: resampling, registration, mouse I/O (functions `imread`, `imagesc`, `ginput`);
- 3D Delaunay triangulation or tetrahedralization, constrained and unconstrained 2D Delaunay triangulations (`delaunay`, `triangulation`);
- 3D surface mesh generation via a sculpting based volumetric method [9] or a region-growing surface method – the ball-pivoting method [10] (via the excellent function `MyRobustCrust` by Dr. L. Giaccari);
- 3D surface-preserving mesh decimation (via the function `reducepatch`);
- Interactive mesh processing tools such as selection of vertices or triangles of a 3D surface mesh and visualization of multiple meshes in many different formats (via the function `select3d` by Dr. J. Conti).

Based on these features, we have established a segmentation workflow entirely in MATLAB. The workflow is illustrated in Fig. 1 and includes:

- Data acquisition (scan data) of the body in the xy-plane using one of a set of images;
- Manual mouse selection of nodes indicating a boundary of interest (segmentation) using 2D mouse input `ginput`. Left click adds a nodal point; right click deletes the previous node, hitting return acquires the next image;

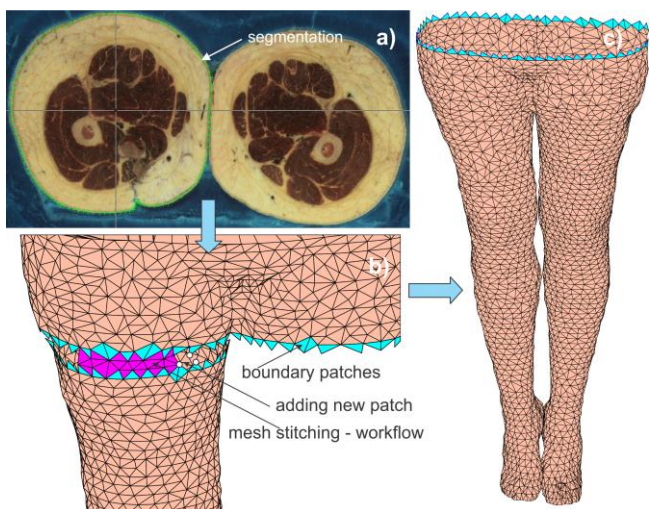


Fig. 1 Illustration of the segmentation/mesh generation workflow: a) – segmentation; b) – stitching of two individual surface meshes; c) – semi-complete surface mesh

- 3D surface mesh generation via the ball-pivoting method as implemented in the function `MyRobustCrust`;
- Automatic selection and visualization of edges with only one adjacent triangle (hole boundaries) and with more than two adjacent triangles (non-manifold edges);
- Sequential selection of individual triangles/nodes/edges using function `select3d`. Manual removal/addition of selected triangles, mesh stitching, mesh healing;
- Mesh smoothing and mesh coarsening using `reducepatch`.

IV. MESH INTERSECTION ALGORITHM IN MATLAB[®]

An important problem is related to intersections of meshes describing different tissues after surface reconstruction. We were unable to find public-domain MATLAB codes that implement one of the existing intersection algorithms [11]-[16]. An original algorithm has therefore been developed and tested. In contrast to the classic paper [11] and other relevant sources [12], [13], [16], we do not explicitly construct the chains and loops of intersection line segments. Instead, all individual intersection line segments are collected randomly and then a constrained 2D Delaunay triangulation is applied to each triangle with the intersection line segments separately. Note that the constrained 2D Delaunay triangulation was also used in [16], but augmented with the construction of intersection chains. The algorithm steps are as follows [17]:

- For each triangle of the master mesh under question, we find intersecting edges $e_i, i = 1, 2, 3, \dots$;
- Next, we apply a constrained 2D Delaunay triangulation to the triangle's plane and subdivide the master triangle into sub-triangles, which respect intersections;
- The same procedure is applied to each triangle under question within the slave mesh;
- We construct refined master and slave meshes, which respect all intersections;
- Boolean operations on meshes are then performed by checking the in/out status of separate triangles.

The above algorithm in its present form is straightforwardly programmed in MATLAB and shows a high reliability. It produces an exact representation of any curved intersecting surfaces. At the same time, it is yet to be optimized for speed and for handling of some degenerate cases. Fig. 2 shows a mesh intersection example. Fig. 2a indicates two intersecting meshes: white matter and CSF ventricles. Fig. 2b shows coincident faces created for both meshes after the intersection

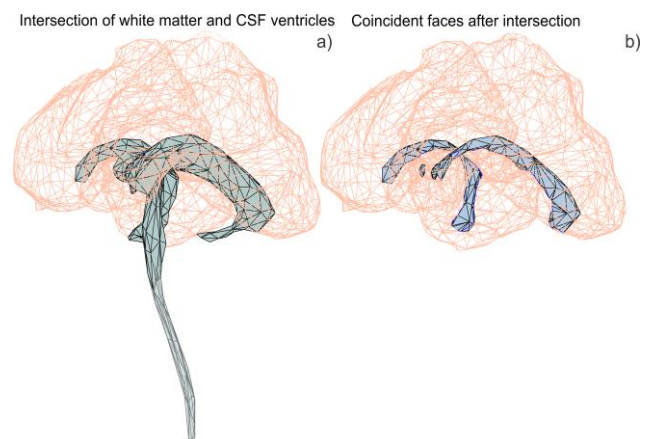


Fig. 2 Image intersection results for white matter and CSF ventricles meshes.

algorithm completes and simultaneously the white matter mesh after subtraction.

V. VHP FEMALE PHANTOM TO DATE

Using the algorithm described above, we have treated multiple intersection cases such as inflated lungs/ribcage,

white matter/CSF ventricles, etc. As a validation step, all meshes have passed the ANSYS High Frequency Structural Simulator (HFSS) mesh check at the strictest setting. Fig. 3 shows the current version of the VHP-Female model with over 80 parts. Ongoing work to augment the phantom is underway.

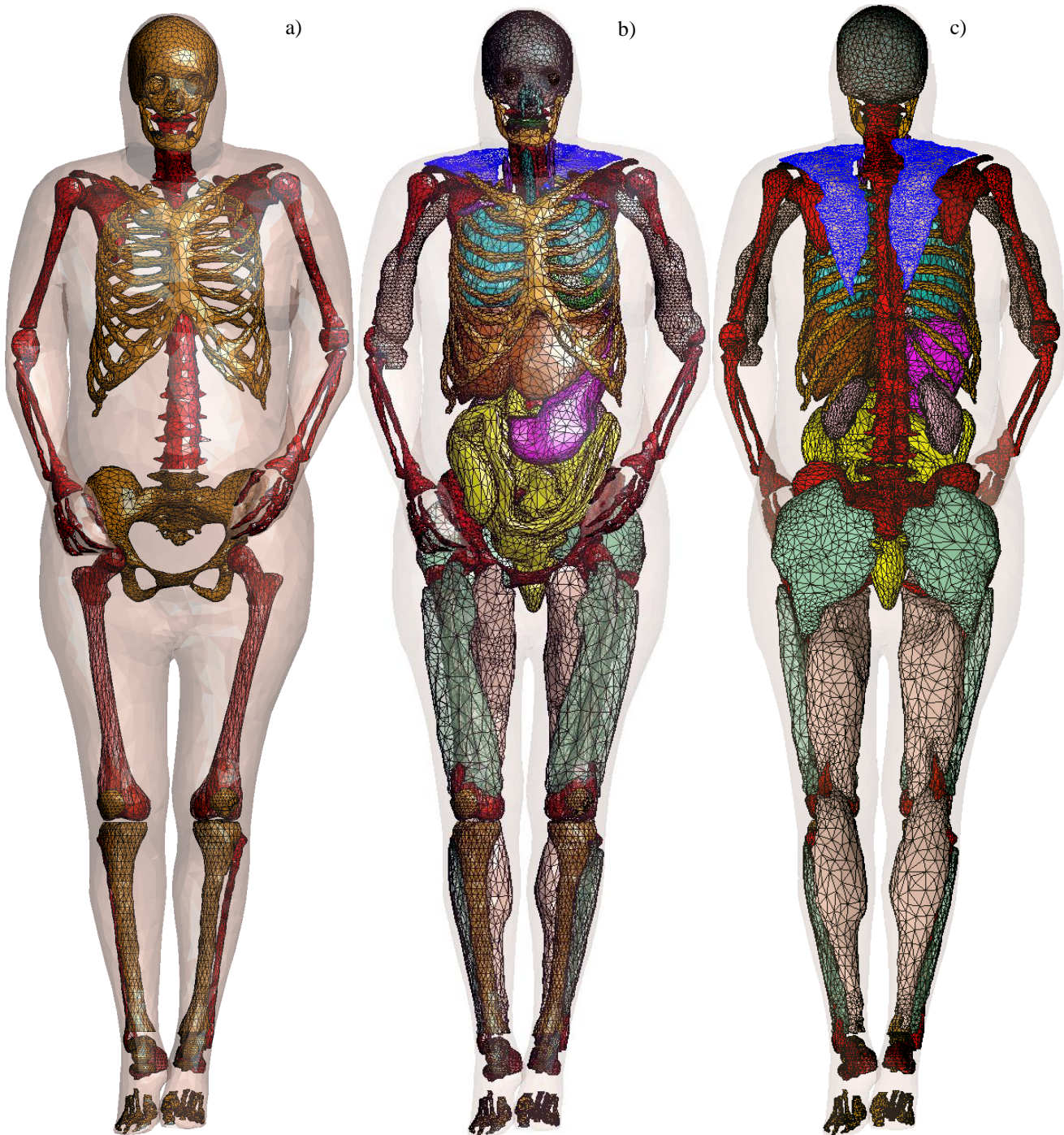


Fig. 3 Partial VHP-Female model to date: a) – skeleton bones, b) – anterior view of organs and muscles, c) – posterior view of organs and muscles.

VI. APPLICATIONS FOR BIOMEDICAL ELECTROMAGNETIC MODELING

The VHP Female phantom has recently been used for modeling Transcranial Direct Current Stimulation (tDCS) with cephalic and extracephalic montages [18]. Static electromagnetic simulations were conducted using ANSYS' Maxwell 3D version 16 product. A wealth of research on the material properties is available [19]-[21] demonstrating the variability of values across multiple types of tissues. It has been shown that extracephalic montages might create larger total current densities in deeper brain regions, specifically in white matter as compared to an equivalent cephalic montage. Extracephalic montages might also create larger average vertical current densities in the primary motor cortex and in the somatosensory cortex. At the same time, the horizontal current density either remains approximately the same or decreases. The metrics include either the total local current density through the entire brain volume or the average vertical and horizontal current densities for each individual lobe/cortex.

The VHP Female phantom has recently been used for RF modeling of CW fields around and within the human head [22]. The following problem has been addressed: find the ideal radio-frequency path through the brain for a given receiver position located on the top of the sinus cavity. The two parameters, transmitter position and radiating frequency, should be optimized simultaneously such that (i) the propagation path through the brain is the longest; and (ii) the received power is maximized. To solve this problem, we have performed a systematic and comprehensive study of the electromagnetic fields excited in the head by small on-body magnetic dipoles (coil antennas). The base radiator is constructed of two orthogonally oriented magnetic dipoles excited in quadrature, which enables us to create a directive beam into the head, as this novel antenna type generates a beam at 45 degrees into a dielectric interface. The CSF and ventricles inside the head form what approximates a dielectric waveguide to channel this beam into the sinus cavities. We have found at least one optimum solution. This solution implies that a distinct RF channel may be established in the brain at a certain frequency and transmitter location. In addition to microwave tomography of the human body, such an antenna can potentially be used to screen for detrimental conditions such as Alzheimer's disease.

Other very recent applications of the VHP-Female model, including the simulation of electrode voltage/current response to CSF pulsations in Rheoencephalography [23], will be presented.

ACKNOWLEDGMENT

We would like to acknowledge the contributions of Mr. A. T. Htet, Mr. J. M. Elloian, and Ms. V. Karna.

REFERENCES

- [1] U.S. National Library of Medicine, The Visible Human Project®, Online: http://www.nlm.nih.gov/research/visible/visible_human.html.
- [2] P. A. Yushkevich, J. Piven, H. C. Hazlett, R. G. Smith, S. Ho, J. C. Gee, G. Gerig, User-guided 3D Active Contour Segmentation of Anatomical Structures: Significantly Improved Efficiency and Reliability, *NeuroImage*, vol. 31 (2006) 1116-28.
- [3] Online: <http://meshlab.sourceforge.net>.
- [4] M. Garland, *Quadric-Based Polygonal Surface Simplification*, PhD Thesis, Pittsburgh, PA, 1999.
- [5] J. Vollmer, R. Mencl, H. Mueller, Improved Laplacian smoothing of noisy surface meshes, *Eurographics*, vol. 18 (1999) 1-8.
- [6] M. Kazhdan, M. Bolitho, H. Hoppe, Poisson Surface Reconstruction, *Eurographics Symposium on Geometry Processing*, 2006.
- [7] G.M. Noetscher, The VHP-F Computational Phantom and its Applications for Electromagnetic Simulations, PhD Thesis, Worcester Polytechnic Institute, Apr. 2014, 307 p.
- [8] IEEE International Committee on Electromagnetic Safety: Technical Committee 34: List of approved human phantoms, Online: <http://groupier.ieee.org/groups/scc34/sc2/wg2/available%20human%20models.doc>.
- [9] C. Bajaj, F. Bernardini, G. Xu, Automatic reconstruction of surfaces and scalar fields from 3D scans, *Computer Graphics Proceedings*, 1995, Annual Conference Series. Proceedings of SIGGRAPH 95, pp. 109-118.
- [10] Bernardini, F., Mittleman, J., Rushmeier, H., Silva, C., Taubin, G., The ball pivoting algorithm for surface reconstruction, *IEEE Trans. Visualization and Computer Graphics*, vol. 5, no 4 (Oct-Dec. 1999).
- [11] S. H. Lo, Automatic mesh generation over intersecting surfaces, *Int. J. Numerical Methods Eng.*, vol. 38 (1995) 943-954.
- [12] S. H. Lo and W. X. Wang, A fast robust algorithm for the intersection of triangulated surfaces, *Engineering with Computers*, vol. 20 (2004) 11-21.
- [13] A. H. Elsheikh, M. Elsheikh, A reliable triangular mesh intersection algorithm and its application in geological modelling, *Engineering with Computers*, vol. 30 (2014) 143-157.
- [14] L. C. Coelho, M. Gattass, L. H. De Figueiredo, Intersecting and Trimming Parametric Meshes on Finite-Element Shells, *Int. J. for Numerical Methods in Engineering*, vol. 0(0) (1999) 1-100.
- [15] W. M. Lira, L. C. G. Coelho, L. F. Martha, Multiple Intersections of Finite-Element Surface Meshes, 11th International Meshing Roundtable, Ithaca, New York, USA, Sep. 15-18, 2002.
- [16] C.H. Lindenbeck, H.D. Ebert, H. Ulmer, L. Pallozzi Lavorante, R. Pflug, TRICUT: a program to clip triangle meshes using the rapid and triangle libraries and the visualization toolkit, *Computers & Geosciences*, vol. 28 (2002) 841-850.
- [17] J. Yanamadala, V. K. Rathi, S. Maliye, H. A. Win, A. L. Tran, M. K. Kozlov, G. M. Noetscher, A. Nazarian, and S. N. Makarov, Segmentation of the Visible Human Project® (VHP) Female Cryosection Images within MATLAB® Environment, 23rd International Meshing Roundtable (IMR23), London, England, Oct. 12-15, 2014.
- [18] G. M. Noetscher, J. Yanamadala, S. N. Makarov, A. Pascual-Leone, Comparison of cephalic and extracephalic montages for Transcranial Direct Current Stimulation - A numerical study, *IEEE Trans. Biomedical Engineering*, vol. 61, no. 9 (Sep. 2014), pp. 2488-2498.
- [19] C. Gabriel, S. Gabriel, E. Corthout, "The Dielectric Properties of Biological Tissues: I. Literature Survey", *Phys. Med. Biol.*, vol. 41, pp. 2231-2249, 1996.
- [20] S. Gabriel, R.W. Lau, C. Gabriel, "The Dielectric Properties of Biological Tissues: II. Measurements in the Frequency Range 10 Hz to 20 GHz," *Phys. Med. Biol.*, vol. 41, pp. 2251- 2269, 1996.
- [21] *IT'IS Material Property Database*, Retrieved Oct. 2nd 2013 from <http://www.itis.ethz.ch/itis-for-health/tissue-properties/overview/>
- [22] J.M. Elloian, G.M. Noetscher, S.N. Makarov, A. Pascual-Leone, Continuous wave simulations on the propagation of electromagnetic fields through the human head, *IEEE Trans. Biomedical Engineering*, vol. 61, no. 6 (June 2014) 1676-1683.
- [23] M. Bodo, Studies in Rheoencephalography (REG, *J Electr Bioimp*, vol. 1, (2010) 18-40.